European Journal of Pharmaceutical Sciences 218 (2026) 107426

Contents lists available at ScienceDirect

European Journal of Pharmaceutical Sciences

journal homepage: www.elsevier.com/locate/ejps

Impact of cocrystal dissolution-supersaturation-precipitation (DSP) behaviour on drug permeation across the PermeaPad® biomimetic barrier

Lucy May Newman [a], Matteo Guidetti [b], Annette Bauer-Brandl [b], Naír Rodríguez-Hornedo [c], Tatiane Cogo Machado [d,*]

[a] School of Pharmacy, Newcastle University, United Kingdom
[b] Department of Physics, Chemistry and Pharmacy, University of Southern Denmark, Denmark
[c] Department of Pharmaceutical Sciences, College of Pharmacy, University of Michigan, USA
[d] School of Mathematical and Physical Sciences, Faculty of Science, University of Technology Sydney, Australia

ARTICLE INFO

Keywords:
Cocrystal dissolution
Supersaturation
Permeation
PermeaPad®
Coformer

ABSTRACT

The purpose of this study was to evaluate how the dissolution-supersaturation-precipitation (DSP) behaviour of cocrystals translates into drug permeation, employing the biomimetic PermeaPad® barrier in a side-by-side cell set-up. Building on our previous work, which demonstrated that reducing an unnecessarily high cocrystal solubility advantage (SA = $S_{cocrystal}/S_{drug}$) through the generation of non-stoichiometric solution conditions can significantly extend the drug supersaturation, we now investigate this approach in the presence of an absorptive environment. Our findings with the 1:1 ketoconazole (KTZ) -*p*-aminobenzoic acid (PABA) cocrystal indicate the existence of an optimal SA value (7), where KTZ-PABA dissolution performance resulted in 8-fold AUC increase, translating to a 7-fold increase in cumulative KTZ permeation after 6 h. This enhancement was achieved by dissolving cocrystal (based on the drug therapeutic dose) with an additional coformer solid phase, rationally designed using a graphical approach grounded in the cocrystal thermodynamic (K_{sp}, $S_{cocrystal}$, S_{drug}) and kinetic parameters (σ_{crit}). The strategy presented in this work can be readily applied during the pre-formulation stage of cocrystal development, enabling targeted selection of coformer concentrations for formulation development. Overall cocrystals offer unique flexibility as a formulation strategy for poorly water-soluble drugs, allowing for tailored DSP behaviour and drug transport over biological barriers based on mechanistic understanding, as demonstrated in this study.

List of abbreviations

ACN	Acetonitrile
API	Active pharmaceutical ingredient
AUC	Area under the curve
A/V	Area to volume ratio
C_{dose}	Dose concentration
C_{max}	Maximum concentration
$[CF]_{Scc}$	Coformer concentration to reach cocrystal solubility at the critical nucleation concentration
$[D]_n$	Critical nucleation concentration
DSC	Differential scanning calorimetry
DSP	Dissolution-supersaturation-precipitation
D/P	Dissolution-permeation
FaSSIF	Fasted state simulated intestinal fluid
HPLC	High-performance liquid chromatography
KTZ	Ketoconazole
PABA	*p*-aminobenzoic acid
RAUC	Relative area under the curve
SA	Solubility advantage
S_{drug}	Drug solubility
$S_{cocrystal}$	Cocrystal solubility
TFA	Trifluoroacetic acid
t_{max}	Time at which the maximum concentration of drug is achieved
TPGS	Tocopherol polyethylene glycol succinate
UHPLC	Ultra-high-performance liquid chromatography
XRPD	X-ray powder diffraction
σ_{max}	Maximum supersaturation
σ_{crit}	Critical supersaturation

* Corresponding author.
E-mail address: tatiane.machado@uts.edu.au (T.C. Machado).

https://doi.org/10.1016/j.ejps.2025.107426
Received 9 November 2025; Received in revised form 9 December 2025; Accepted 31 December 2025
Available online 1 January 2026

1. Introduction

The interplay between dissolution and precipitation of supersaturating formulations has been extensively investigated, with significant advances made for enabling formulations such as amorphous solid dispersions (ASD), lipid-based systems and cocrystals. (Fong et al., 2017; Kuminek et al., 2016; Schver and Lee, 2018; Stillhart and Kuentz, 2016; Sun and Lee, 2015) For pharmaceutical cocrystals, deeper understanding of the mechanistic aspects of dissolution–supersaturation–precipitation (DSP) behaviour has emerged based on stoichiometric composition and thermodynamic properties, highlighting the influence of solution conditions such as dose, pH, and additives including lipids and polymers. (Machado et al., 2020, 2022) In our recent study of the 1:1 ketoconazole–*p*-aminobenzoic acid (KTZ–PABA) cocrystal, the impact of excess non-stoichiometric coformer concentrations on drug supersaturation performance (DSP) was evaluated, demonstrating the usefulness of a conceptual phase diagram for selecting coformer concentrations tailored to specific cocrystal doses to extend the drug's supersaturation lifetime. (Newman et al., 2025) Thus, the mechanisms underlying cocrystal DSP have been well characterized, in contrast to other types of enabling formulations. However, a significant gap remains with respect to whether these mechanisms would increase drug transport over biological barriers accordingly, with limited studies assessing cocrystal performance under *in vitro* absorptive conditions. (Guo et al., 2018; Pandey and Ghosh, 2022; Sanphui et al., 2015) Most investigations employ single-compartment dissolution apparatus and classical analytical methods which do not account for free (absorbable) drug fractions in biomimetic media, raising important questions as to how cocrystals perform in absorptive environments to mimic *in vivo* situations. (Buckley et al., 2013)

Advances in biopharmaceutical technology mean today's pharmaceutical scientist has many options to integrate dissolution and permeation studies in cocrystal development. (O'Shea et al., 2022) *In vitro* instrumentation such as Ussing chambers, 96-well plates, Franz cells and side-by-side cells accompanied by biological barriers including Caco-2 cells or artificial membranes to replicate intestinal epithelium are of the most common. Cell-free permeation tools, such as the biomimetic PermeaPad® barrier, provide a more sustainable alternative to cell-based models, offering greater cost-efficiency and reproducibility. (Di Cagno et al., 2015; Jacobsen et al., 2023) Comprised of immobilized phosphatidylcholine vesicles sandwiched between two cellulose hydrate support sheets, the PermeaPad® barrier has been utilized in studies investigating ASD's, lipid-based systems and other supersaturating formulations such as pH modulated granules and suspensions. (Bibi et al., 2017; Eriksen et al., 2020; Holzem et al., 2022, 2023; Ilie et al., 2020; P. D. Nunes, Pinto, et al., 2023) Despite the range of experimental models available, combined *in vitro* dissolution-permeation (D/P) studies of cocrystals remain few in numbers. (Dai et al., 2016; Guo et al., 2018; Sanphui et al., 2015) Most recently, Guidetti et al., employed the PermeaPad® barrier in the 96-well plate format to successfully investigate posaconazole cocrystals, reporting a 4–5-fold improvement in drug permeation compared to the pure crystalline drug form. (Guidetti, 2024)

Building on our previous publication (Newman et al., 2025), which investigated the dissolution of KTZ-PABA in fasted state simulated intestinal fluid (FaSSIF) with varying stoichiometric concentrations of coformer under USP apparatus 2 (without an absorptive sink), we now extended our studies to investigate the dynamics of dissolution and permeation together, using a side-by-side diffusion cell system separated by the biomimetic PermeaPad® barrier. Excess PABA concentrations 2.59, 5.17 and 10.34 mM were analysed in our previous study and are further assessed in the current manuscript.

Our overarching goal is to demonstrate the value of combined *in vitro* D/P studies to provide insights into the kinetic contributions of cocrystal dissolution to drug permeation, into more physiologically meaningful contexts. To this end, it is studied whether extended cocrystal supersaturation, achieved by addition of excess coformer, will enhance the amount of drug permeated and thereby suggest improved *in vivo* absorption. In addition, we highlight critical considerations for experimental design, including identification of key parameters for the rational coformer and cocrystal dose selection and comprehensive thermodynamic characterization of cocrystals.

2. Materials and methods

2.1. Materials

2.1.1. Cocrystal components

Ketoconazole (KTZ) was purchased from Thermo Fisher Scientific chemicals (Cramlington, UK) and *p*-aminobenzoic acid (PABA) was purchased from Fluorochem (Hadfield, UK). Drug and coformer were characterised by X-ray powder diffraction (XRPD) prior to experiment execution.

2.1.2. Solvents and reagents

Acetonitrile (ACN) was purchased from VWR International (Søborg, Denmark). Trifluoroacetic acid (TFA) was purchased from Fisher Scientific (Roskilde, Denmark). Fasted state intestinal fluid (FaSSIF) buffer concentrate and FaSSIF/FeSSIF/FaSSGF 3F powder were acquired from Biorelevant (London, UK). Sodium chloride (NaCl) was purchased from Sigma-Aldrich (St. Louis, USA). Ultrapure Milli-Q water (resistivity 18.2 MΩ·cm at 25 °C; total organic carbon (TOC) $\leq$ 2 ppb) was prepared in the laboratory and used for all buffer preparations. Vitamin E tocopherol polyethylene glycol succinate (Vit E TPGS) was a kind gift of Gustav Parmentier GmbH (Frankfurt, Germany).

2.1.3. Prepared media reagents

FaSSIF media were prepared by dissolving the appropriate amount of FaSSIF buffer concentrate and FaSSIF/FeSSIF/FaSSGF 3F powder in Ultrapure Milli-Q water, according to manufacturer protocols (Biorelevant.com Ltd., UK). To prepare 1 L of FaSSIF medium, 41.65 g of FaSSIF buffer concentrate and 2.24 g of FaSSIF/FeSSIF/FaSSGF 3F powder were dissolved in Ultrapure Milli-Q water and allowed to equilibrate for 2 h. Blank FaSSIF was prepared as above, with the exclusion of the 3F powder. The pH of each medium was adjusted to 6.50 with 1 M NaOH. Media were stored at room temperature and used within 48 h of preparation.

A suitable acceptor medium is crucial to overcome challenges to quantify low concentrations in the acceptor compartment, by maintaining a sufficient affinity to increase the rate of permeation while maintaining sink conditions to prevent any influence on permeation flux. A preliminary study was conducted to determine an appropriate medium and is further detailed within the supplementary material (Section 2). The selected acceptor medium contained 4 g of Vit E TPGS in 200 mL of blank FaSSIF pH 6.50, resulting in a 2 % w/v Vit E TPGS in Blank FaSSIF pH 6.50 solution. Vit E TPGS increases drug solubility in the acceptor compartment, ensuring the drug concentrations were detectable and quantifiable, whilst maintaining sink conditions. The PermeaPad® barrier is designed to permit the diffusion of drug molecules, while restricting larger surfactant molecules including Vit E TPGS, preventing back permeation from the acceptor into the donor compartment.

The osmolalities of donor and acceptor media were determined (OSMOMAT 030-D osmometer, Gonotec, Germany) and adjusted by dissolving a sufficient quantity of NaCl to be within $\pm$ 5 % of each other, avoiding a high osmotic gradient. Initial pH and osmolality for donor and acceptor media in each study are recorded within the supplementary material. (Table S7)

2.2. Methods

2.2.1. Cocrystal preparation

The 1:1 KTZ-PABA cocrystal was prepared by reaction crystallisation method (RCM) at room temperature by adding KTZ to a nearly saturated solution of PABA in ACN. (Rodríguez Hornedo Naír et al., 2006) KTZ-PABA was prepared by adding 751.6 mg of PABA and 2953.6 mg of KTZ to 45 mL of ACN. Suspensions were stirred for 24 h and filtered under vacuum. Stoichiometric purity was verified by HPLC after dissolving a known amount of cocrystal in HPLC diluent, and quantifying the molar ratio of drug and coformer using calibration curves determined from pure substances. Cocrystal solid phase was characterised by XRPD and differential scanning calorimetry (DSC). (Fig. S2 and Fig. S3) Full conversion to cocrystal was observed within 24 h. Diagram showing cocrystal formation pathway is added to the supplementary material. (Fig. S1)

2.2.2. Cocrystal and drug thermodynamic solubility measurements

Cocrystal and drug solubilities were measured at the eutectic point in which drug and cocrystal solid phases are in equilibrium with the solution. (Rodríguez Hornedo Naír et al., 2006) KTZ and KTZ-PABA solubilities were determined in the selected donor medium of FaSSIF pH 6.50 with experimental methodology and results, previously reported in our most recent publication. (Newman et al., 2025) (Table 1) To ensure sink conditions in the D/P set up, drug solubility in the acceptor media was conducted as part of the preliminary study and newly obtained data is documented within section 2.3 of the supplementary material.

2.2.3. Graphical approach for the phase diagram

From a single experimental measurement of a cocrystal and drug eutectic point combined with knowledge of cocrystal stoichiometry, a log [Drug] *vs* log [Coformer] phase diagram (Fig. 1 and Fig. 3) was constructed to show regions over which cocrystal dissolution and drug precipitation can be modulated. (Machado et al., 2022; Newman et al., 2025) Intersecting at the eutectic point, the cocrystal solubility ($S_{cocrystal}$) line has a slope of −1 for a cocrystal of 1:1 stoichiometry and under the same experimental conditions $S_{drug} = [Drug]_{eu}$. The mass of cocrystal corresponds to a dose concentration (C_{dose}) which, for a cocrystal with 1:1 stoichiometry, drug and coformer C_{dose} are equal. In the present work a C_{dose} of 1.51 mM was selected based upon a KTZ marketed dose of 200 mg and a luminal volume of 250 mL. The critical concentration for drug nucleation ($[D]_n$) was determined from the maximum drug concentration (C_{max}) observed in the current D/P studies. $[CF]_{Scc}$ is the coformer concentration required to reach cocrystal solubility at the critical supersaturation and is drawn at the intersection of $[D]_n$ and $S_{cocrystal}$.

2.2.4. Combined dissolution/permeation studies

D/P studies of pure drug and cocrystal with and without excess PABA were conducted in a side-by-side cell (PermeGear Inc., Hellertown, PA, USA) set-up as depicted in Fig. 2. (PermeGear Inc., Hellertown, PA, USA) Donor and acceptor compartments were filled with 7 mL of FaSSIF pH 6.50 and 5 mL 2 % w/v Vit E TPGS pH 6.50, respectively. Each compartment was separated by an artificial biomimetic PermeaPad® barrier (Phabioc, Karlsruhe, Germany) and two rubber O-rings to ensure each chamber remained sealed. A surface area of 1.75 cm^2 was available for permeation, corresponding to an area-donor volume (A/V) ratio of 0.25 cm^{-1}. Compartments were maintained at 37 °C using a water jacket and stirred under a fixed speed of 500 rpm (H-3 stirrer, PermeGear Inc., Hellertown, PA, USA). Addition of 1.51 mM KTZ-PABA with and without excess PABA concentrations (2.59, 3.88, 5.17, 7.76 and 10.34 mM) were directly added to each donor vessel using folded weighing paper as a funnel. (Fig. S4) PABA concentrations of 2.59, 5.17 and 10.34 mM had previously been assessed in our most recent manuscript. (Newman et al., 2025) To characterise DSP behaviour and the influence of an absorptive sink, a further two additional coformer concentrations (3.38 and 7.76 mM PABA) were also evaluated. Prior to analysis, KTZ-PABA and excess PABA powders were sieved via a 120 µm mesh. (Micro sieve, Sigma-Aldrich) For D/P studies performed with additional coformer, the KTZ-PABA and PABA powders were thoroughly mixed in an agate mortar and pestle before the experiment. To represent an oral dosage form, excess coformer concentrations were added in solid state simultaneously with the cocrystal solid dose. Such concentrations of PABA do not naturally exist *in vivo*, therefore, introducing pre-dissolved coformer would not be representative. The pH of donor and acceptor media was measured for each studied condition prior to solid phase addition and after the final aliquot was removed at the 6 h timepoint. Aliquots of 200 µL were withdrawn from the donor compartment at pre-determined timepoints and filtered through a 0.1 µm Anotop® syringe filter. Acceptor samples of 200 µL were collected at various timepoints. Each aliquot was appropriately diluted and concentrations of drug and coformer determined by HPLC or UHPLC. Each compartment was replenished with 200 µL of fresh medium. At the end of the experiment, the remaining suspensions in the donor compartments were collected using a Pasteur pipette, transferred to a centrifuge tube filter (Corning Costar Spin X®, Corning, Salt Lake City, United States) with a 0.45 µm cellulose acetate membrane. Suspensions were centrifuged at 10,000 rpm for 2 min to isolate the solid phase. Collected solid phase was incubated at 37 °C for 2 h before characterisation by XRPD. All conditions tested were performed in triplicate.

2.2.5. High-performance liquid chromatography (HPLC)

KTZ and PABA donor concentrations were quantified using a Waters 2695 D separation module coupled with a 2487 dual absorbance detector (Waters Corporation Milford, MA, USA) and a reverse phase Atlantis T3 C18 column (5 µm, 250 × 4.6 mm) maintained at 25 °$C \pm 0.1$ °C. The mobile phase consisted of ACN and 0.1 % TFA in water using a gradient elution beginning at a proportion of 40:60 and ending at 60:40 (ACN:0.1 %TFA in H_2O). A sample injection volume of 20 µL and flow rate of 0.85 mL/min were employed. Diluent composition was 40:60 (ACN:0.1 %TFA in H_2O). KTZ and PABA were quantified at 240 nm and eluted at 5.9 min and 4.0 min, respectively.

Table 1
Key thermodynamic parameters for 1:1 KTZ-PABA cocrystal: $S_{cocrystal}$, SA, K_{sp} and $K'_{sptotal}$ obtained from the measured $[KTZ]_{eu,T}$ and $[PABA]_{eu,T}$ at equilibrium with drug and cocrystal solid phases in FaSSIF. T refers to total concentrations comprising of all drug and coformer species (ionised and micellar). Equilibrium was achieved between 72 h – 96 h.

	$[KTZ]_{eu,T}$ (mM)	$[PABA]_{eu,T}$ (mM)	$S_{cocrystal,T}$ (mM)	SA = $S_{cocrystal}/S_{drug}$	$K'_{sptotal}$ (mM^2)	K_{sp} (mM^2)
Experimental value at equilibrium pH 5.82 ± SD [a]	0.089 ± 0.001	11.852 ± 0.110	1.029 ± 0.006 [b]	12	1.060 ± 0.012 [c]	4.744 (± 0.237) x 10^{-5} [d]

[a] Data obtained in previous study (Newman et al., 2025).

[b] $S_{cc,T} = \sqrt{[drug]_{eu,T}\,[coformer]_{eu,T}}$.

[c] K_{sp}'$_{total}$ was experimentally determined from the eutectic analytical concentrations according to K_{sp}'$_{total} = [D]_{T,eu}[CF]_{T,eu}$.

[d] K_{sp} is calculated as the product of the constituent concentrations in the same molecular state as the cocrystal (*i.e.* neutral), according to $K_{sp} = [KTZ]_0[PABA]_0$. The subscript 0 indicates the neutral state of drug or coformer. Non-ionised species were calculated from $[KTZ]_{eu,T}$ and $[PABA]_{eu,T}$ by rearranging solubility equations as detailed in the supplementary material (Section 3).

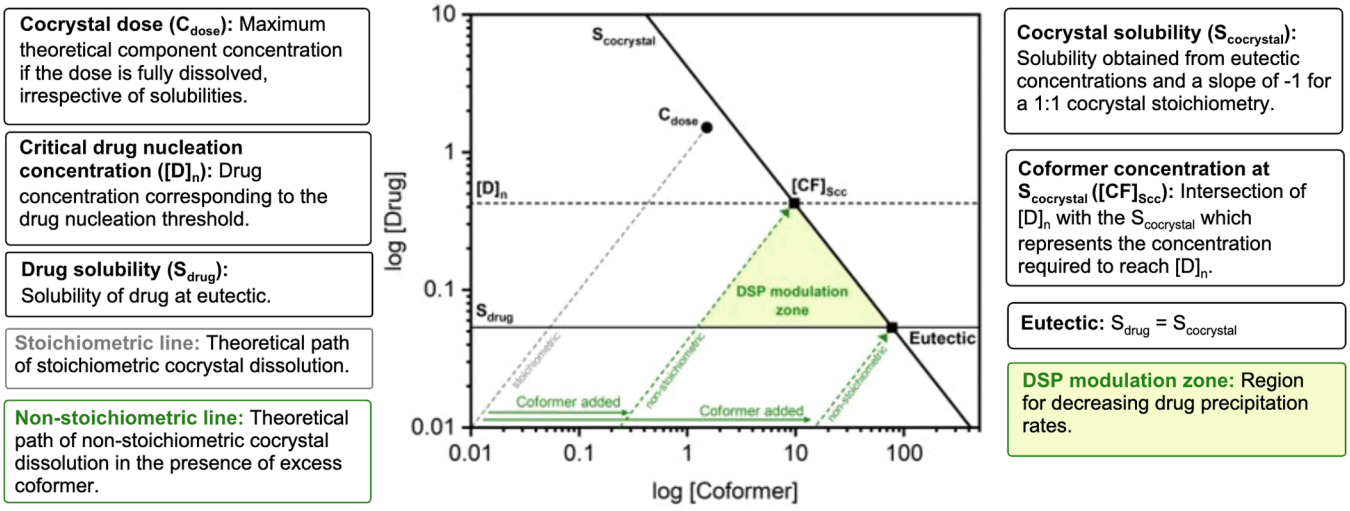

Fig. 1. Schematic diagram for cocrystal phase diagram construction, depicting thermodynamic ($S_{cocrystal}$ and S_{drug}) and kinetic ($[D]_n$) parameters. The shaded green region depicts the zone in which drug supersaturation may be generated and sustained by addition of excess coformer. Coformer non-stoichiometric conditions are represented by the green dashed arrows.

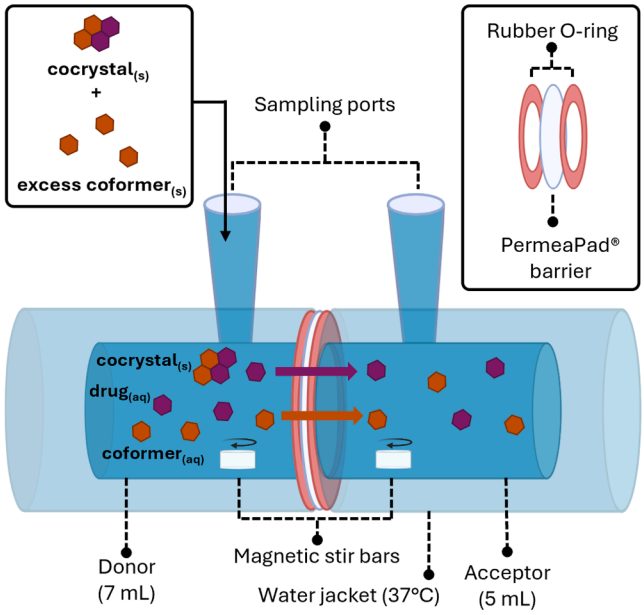

Fig. 2. Diagram depicting the side-by-side cell set up for this study, comprising of a donor and an acceptor cell separated by rubber O-rings and the PermeaPad® barrier. Schematic representation of cocrystal dissolution in the donor compartment and permeation of drug and coformer into the acceptor side. Physical states are indicated by (aq) for aqueous and (s) for solid.

2.2.6. Ultra-high performance liquid chromatography (UHPLC)

The UHPLC ultraviolet system (Thermo Fisher Scientific, Massachusetts, USA) consisted of an UltiMate® Rapid Separation Autosampler (WPS-3000RS), UltiMate® Rapid Separation Thermostatted Column compartment (TCC-3000RS) and an UltiMate® Rapid Separation UHPLC Diode Array Detector (DAD-3000RS). A Kinetex EVO—C18 100A column (1.7 µm, 150 × 2.1 mm) (Waters, Milford, USA) was employed for UHPLC-UV analysis. An isocratic method was employed for the quantification of KTZ in the acceptor compartment with a mobile phase consisting of 35 % ACN and 65 % 0.1 % TFA in H_2O (v/v) proportion and a run time of 3 min. Column temperature was maintained at 25 °C ± 0.1 °C for the duration. A flow rate of 0.25 mL/min, injection volume of 5 µL and detection wavelength of 230 nm were applied. The KTZ peak eluted at 2.2 min.

2.2.7. X-ray powder diffraction (XRPD)

Diffractograms were obtained using a Rigaku Miniflex600 (Rigaku Corporation, Tokyo, Japan) equipped with a scintillation (NaI) counter detector with a Θ/2Θ geometry. Operating with a copper K_α radiation at a current of 15 mA and a voltage of 40 kV. The measurements were performed at room temperature, scanning at 2Θ from 2° to 40°, with a 0.02°2Θ step size at a speed of 5°2Θ/min. Results were compared to diffraction patterns calculated from crystal structures reported in Cambridge Structural Database (CSD). KTZ-PABA cocrystal identification code is IRIBET. (Groom et al., 2016; Martin et al., 2020)

3. Results and discussion

3.1. Cocrystal thermodynamic properties and the phase diagram

KTZ-PABA solubility in FaSSIF pH 6.50 was assessed by measuring drug and coformer concentrations in equilibrium with cocrystal and drug solid phases, which refers to the eutectic point. Concentrations equilibrated at pH 5.82, due to the self-buffering behaviour of PABA, an amphoteric compound with pK_a values of 2.41 and 4.87 (Lukács et al., 1998). The thermodynamic parameters in Table 1, obtained from this single experiment, form the foundation for modulating desirable cocrystal dissolution performance. Particularly, the cocrystal solubility advantage relative to drug (SA = $S_{cocrystal}/S_{drug}$), which indicates the cocrystal potential to generate drug supersaturation. KTZ-PABA exhibits a SA = 12 in FaSSIF at pH 5.82, meaning that it incongruently saturates the dissolution media as supersaturation leads to drug precipitation. However, this does not guarantee that the drug will reach this level of supersaturation during cocrystal dissolution. The actual supersaturation achieved will depend on the critical supersaturation (σ_{crit}) for drug nucleation, which is the practical limit, and other kinetic factors like stirring rate or apparatus type. The general rule applies: the higher the cocrystal SA, the greater the risk of drug precipitation. (Cavanagh et al., 2020)

Cocrystal solubility can be influenced by the presence of solubilizing agents, non-stoichiometric solution composition and pH. (Good and Naír, 2009; Huang et al., 2019) Since KTZ solubility is highly pH-dependent due to its basic nature (pK_{a1} = 3.17 and pK_{a2} = 6.63) (Avdeef, 2012), KTZ-PABA solubility is expected to change with small changes in pH. (Fig S8A) Therefore, to reflect the dissolution medium

conditions (FaSSIF pH 6.50), parameters used to construct the [KTZ] *vs* [PABA] phase diagram were predicted at pH 6.50 (Table 2). Fig. 3A illustrates the phase diagram at eutectic pH 5.82, whilst Fig. 3B represents the diagram at a physiological pH of 6.50, allowing for better visualisation of pH influence. S_{drug} and $[D]_n$ are lower at pH (6.50), due to the ionization behaviour of KTZ, whereas $S_{cocrystal}$ is higher (Fig. S8A). A more detailed phase diagram showing how these parameters change with pH variations encountered in the dissolution studies is shown in Figure S9.

This diagram was previously introduced (Machado et al., 2022; Newman et al., 2025) to determine the metastable zone between drug solubility (S_{drug}) and the critical concentration for nucleation ($[D]_n$), in which the interplay between cocrystal dissolution and drug precipitation can be modulated to promote sustained drug supersaturation, increasing its exposure for permeation. The cocrystal dose to be dissolved (C_{dose}) is plotted to assess whether it can provide cocrystal component concentrations within the metastable zone for modulation (green area in Fig. 3). According to cocrystal K_{sp}, generation of non-stoichiometric coformer concentrations alters the driving force for cocrystal dissolution and drug precipitation, by lowering cocrystal solubility. (Nehm et al., 2006) In this study, we generated non-stoichiometric coformer concentrations by performing dissolutions of the cocrystal C_{dose} (1.51 mM), together with varied excess concentrations of PABA (2.59, 3.88, 5.17, 7.76 and 10.34.mM) with the objective of decreasing cocrystal SA and driving the system toward generating drug concentrations close to critical threshold $[D]_n$, in the intersection with $[CF]_{Scocrystal}$. This trend is evident in the phase diagram (Fig. 3), where increasing coformer concentration leads to a decrease in cocrystal solubility. Consequently, cocrystal solubility advantage over drug ($SA = S_{cocrystal}/S_{drug}$) may be diminished, reducing the driving force for drug precipitation. The full derivation of cocrystal K_{sp} equilibria and its influence on cocrystal solubility is provided in the supplementary material (Section 3). At FaSSIF pH 6.50, KTZ-PABA exhibits a SA = 38, representing a high driving force for drug precipitation. Targeted concentrations of PABA shift the C_{dose} to supply the cocrystal saturation line at different regions (indicated by arrows in Fig. 3), corresponding to lower SA values, which will be discussed in more detail later.

Table 2
Key parameters for the construction of the phase diagram in FaSSIF pH 6.50, including drug and cocrystal solubility (S_{drug} and $S_{cocrystal}$), $[D]_n$, dose concentration (C_{dose}) and K_{sp}'$_{total}$ used for determination of $S_{cocrystal}$ line. Values at the intersection in the phase diagram between $[D]_n$ and $S_{cocrystal}$ which represents $[CF]_{Scocrystal}$, and the intersection of the eutectic between S_{drug} and $S_{cocrystal}$.

Parameter	Value
C_{dose}	1.51 mM
S_{KTZ}	0.053 mM [a]
$S_{KTZ\text{-}PABA}$	2.037 mM [b]
$SA = (S_{cocrystal}/S_{drug})$	38
K_{sp}'$_{total}$	4.149 mM^2 [c]
$[D]_n$	0.428 mM [d]
$[KTZ]_{eu}$	0.053 mM [e]
$[PABA]_{eu}$	77.541 mM [f]
$[KTZ]_{Scc}$	0.428 mM [g]
$[PABA]_{Scc}$	9.692 mM [g]

[a] Obtained from S_{KTZ} predictions (Fig S8A) from KTZ equilibrium solubility in FaSSIF pH 6.50.

[b] Determined from $S_{cocrystal\ (FaSSIF)} = S_{cocrystal\ (aqueous)} \times \sqrt{SR_{drug}}$ where SR is the solubilisation ratio $SR_{drug} = S_{drug\ (FaSSIF)} / S_{drug(aqueous)}$.

[c] Determined considering $K_{sp}'_{total} = K_{sp}\delta^{y}_{D,T}\delta^{z}_{CF,T}$, where δ represents the ionised and solubilised cocrystal components and y, z denote the stoichiometric coefficients. (Machado et al., 2022).

[d] $[D]_n$ corresponds to the KTZ nucleation threshold at $\sigma_{crit} = 8$ and was obtained from the maximum KTZ concentration achieved during pure KTZ-PABA dissolution in FaSSIF in the D/P side-by-side cell.

[e] Under the same conditions, $[KTZ]_{eu} = S_{drug}$.

[f] Determine by $[PABA]_{eu} = K_{sp}'_{total}/[KTZ]_{eu}$.

[g] Corresponds to KTZ and PABA concentrations at the intersection of $[D]_n$ and $S_{cocrystal}$.

3.2. Cocrystal DSP in the presence of an absorptive environment: donor compartment

3.2.1. Drug supersaturation vs time profiles

The high solubility of KTZ-PABA (SA = 38) resulted in faster dissolution and drug precipitation rates for pure cocrystal dissolution in FaSSIF, as illustrated in Fig. 4, which shows the cocrystal DSP in the donor compartment and its dependence on non-stoichiometric coformer concentrations in terms of supersaturation (C_{drug}/S_{drug}) *vs* time profiles. The addition of PABA resulted in varied precipitation kinetics due to the modulation of cocrystal SA. (Fig. 4) In all conditions studied, KTZ-PABA cocrystal generated KTZ supersaturation, except with additional 10.34 mM PABA. De-supersaturation rate is fastest for pure cocrystal, followed by cocrystal with excess 2.59 mM and 3.88 mM PABA. These three conditions exhibited a typical DSP profile, characterised by a sharp increase in drug supersaturation, followed by a decline due to drug precipitation. Differently, a sustained supersaturation performance was observed for cocrystal with the addition of 5.17 mM PABA ($\sigma_{max} = 4.7 \pm 0.6$). This steady-state dissolution is due to synchronization of cocrystal dissolution and drug precipitation, a mechanism previously discussed. (Machado et al., 2022; Newman et al., 2025) Cocrystal with 7.76 mM excess PABA generated KTZ sustained supersaturation but at lower levels ($\sigma_{max} = 2.8$) for the duration of the experiment. In the highest excess PABA 10.34 mM condition, the cocrystal SA was decreased, to a point where there was no meaningful solubility advantage of cocrystal over drug, therefore supersaturation cannot be generated. For pure cocrystal, the SA increases with increasing pH above its pH_{max}. (Fig S8B) As the concentration of PABA added increases, the donor pH decreases (Table 3) leading to an increased S_{KTZ}, therefore supersaturation values were obtained considering the S_{KTZ} at the corresponding final pH to account for this influence. (Fig. S8A)

The area under the curves (AUCs) obtained during cocrystal dissolutions are shown in Table 3. These values represent the drug available for permeation, which for cocrystals, is directly proportional to dissolution and supersaturation and inversely proportional to precipitation. The low AUC exhibited by KTZ-PABA is due to the complete and rapid cocrystal conversion to drug. (Fig. S10A) In contrast, for 2.59, 3.88 and 5.17 mM PABA conditions, the final solid phase consists of a mixture of cocrystal and drug, whilst in conditions with 7.76 and 10.34 mM PABA consisted of cocrystal only. (XRPD in Fig S10) AUC increases as PABA concentration increases up to 5.17 mM PABA, beyond which cocrystal dissolution advantage begins to diminish due to high coformer concentrations added. Fig S12 depicts the component concentrations and trajectory of cocrystal dissolution of each studied condition in the context of the log [drug] *vs* [coformer] diagram.

3.2.2. Correlation between cocrystal solubility advantage (SA) and dissolution outcomes

The influence of the added non-stoichiometric concentrations of PABA on decreasing cocrystal conversion rates can be further examined from the correlation between cocrystal SA and the relative area under the curve ratio ($RAUC = AUC_{cocrystal}/AUC_{drug}$) in Fig. 5. Estimation of cocrystal SA under non-stoichiometric conditions can be directly obtained from the phase diagram, from the ratio of $S_{cocrystal}$ to S_{drug}. (Fig. S12 and Table S6) or by using the equation $S_{cocrystal} = K_{sp}'_{total}/[PABA]_{added} + C_{dose}$, to obtain the $S_{cocrystal}$. The influence of excess coformer on cocrystal solubility was first introduced by (Nehm et al., 2006) and further details on SA determination are documented within

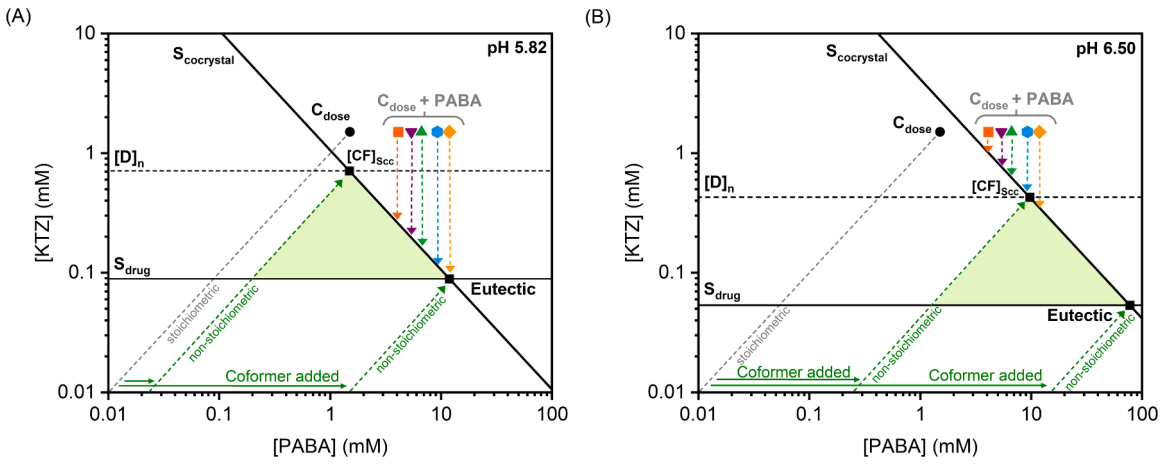

Fig. 3. Diagrams illustrating how cocrystal C_{dose}, and the additional coformer concentrations relate to drug and cocrystal solubility (S_{drug} and $S_{cocrystal}$) and the critical concentration for nucleation ($[D]_n$). The diagram was constructed by considering experimental data from eutectic measurements in FaSSIF at equilibrium pH 5.82 (Table 1) (A) and predictions at pH 6.50 (B), corresponding with experimental D/P study pH (Table 2). The $S_{cocrystal}$ line, with a slope of −1 for a 1:1 cocrystal, was drawn from the data in corresponding tables and passes through the measured eutectic point indicated by the black square. $[D]_n$ corresponds to a critical supersaturation $\sigma_{crit} = 8$ ($\sigma_{crit} = [D]_n / S_{drug}$). Grey dashed line represents theoretical stoichiometric dissolution of cocrystal. Additional PABA concentrations selected for analysis are represented by coloured symbols and correspond to the C_{dose} (1.51 mM) plus the $[PABA]_{added}$. Green area refers to the region of drug supersaturation where nucleation and precipitation rates can be modulated by adding coformer. Non-stoichiometric green dashed lines, show the theoretical pathway for the non-stoichiometric dissolution of cocrystal with additional coformer.

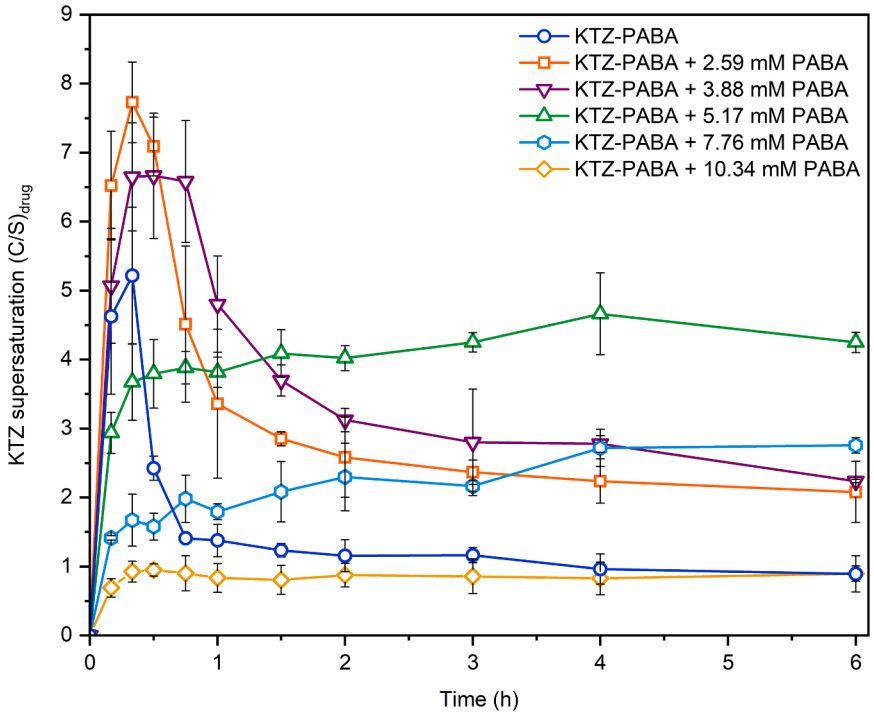

Fig. 4. Drug supersaturation *vs* time profiles, during cocrystal dissolution in donor compartment of side-by-side cells in the presence of an absorptive sink; with and without excess coformer concentrations (2.59, 3.88, 5.17, 7.76 and 10.34 mM) (0–6 h) in FaSSIF pH 6.50. KTZ-PABA exhibited varied supersaturation and precipitation kinetics which are dependent on the non-stoichiometric solution composition. Error bars represent ± standard deviation (SD) ($n = 3$).

the supplementary material. Excess PABA predictably decreases cocrystal SA according to the K_{sp} behaviour. Fig. 5 shows a decrease in SA from 38 (pure KTZ-PABA) to 2 (highest PABA concentration of 10.34 mM). Due to the unnecessarily high SA in FaSSIF, KTZ–PABA rapidly converted to KTZ, resulting in a limited dissolution advantage compared to pure KTZ (RAUC = 2.3 ± 0.3). As PABA is added, an increase in RAUC is observed (5.1 ± 0.6 for 2.59 mM PABA) until it reaches the highest dissolution advantage (RAUC = 8.1 ± 0.4) with the additional 5.17 mM PABA concentration. This indicated that there is an optimal SA (7) value associated with the highest RAUC, which was generated by addition of 5.17 mM PABA. Notably, the 3.88 mM PABA condition also led to a substantial dissolution enhancement, with a 6.3-fold increase in AUC. In both best dissolution performances, SA is modulated to values around 7–10, which are near the KTZ critical supersaturation ($\sigma_{crit} = 8$), yet still provide a significant advantage. In contrast, the excess 7.76 mM and 10.34 mM PABA decreased RAUC to 4.9 ± 0.5 and 1.9 ± 0.2, respectively. Increasing PABA concentration lowers $S_{cocrystal}$ shifting the system towards the eutectic point, in which SA = 1 and cocrystal solubility

Table 3
Dissolution key parameters for pure KTZ and KTZ-PABA with and without excess PABA during combined D/P in the donor compartment, including SD ($n = 3$). Initial FaSSIF pH = 6.50.

Solid phase ($PABA_{added}$)	C_{max} (mM) ± SD	t_{max} (h)	σ_{max} ± SD [a]	$AUC_{donor(0–6 h)}$ (mM.h) ± SD	Final donor compartment pH ± SD [b]
KTZ	0.035 ± 0.002	6	0.6 ± 0.1	0.184 ± 0.007	6.51 ± 0.01
KTZ-PABA (0 mM)	0.278 ± 0.053	0.3	5.2 ± 0.9	0.428 ± 0.059	6.48 ± 0.02
KTZ-PABA (2.59 mM)	0.417 ± 0.032	0.3	7.7 ± 0.6	0.940 ± 0.101	6.34 ± 0.01
KTZ-PABA (3.88 mM)	0.387 ± 0.053	0.5	6.7 ± 0.9	1.160 ± 0.059	6.32 ± 0.01
KTZ-PABA (5.17 mM)	0.281 ± 0.036	4	4.7 ± 0.6	1.496 ± 0.066	6.28 ± 0.01
KTZ-PABA (7.76 mM)	0.177 ± 0.007	6	2.8 ± 0.1	0.902 ± 0.096	6.19 ± 0.01
KTZ-PABA (10.34 mM)	0.072 ± 0.007	0.5	1.0 ± 0.1	0.358 ± 0.042	5.99 ± 0.01

[a] Maximum KTZ supersaturation ($\sigma_{max} = C_{max}/S_{drug}$).
[b] Final refers to 6 h timepoint.

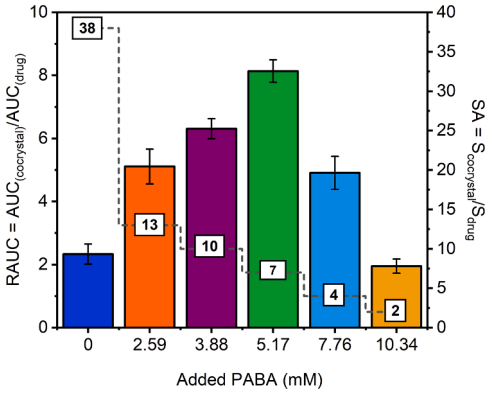

Fig. 5. Dissolution RAUC (0–6 h) ($AUC_{cocrystal}/AUC_{drug}$) and cocrystal SA for each dissolution condition. Dashed line and numbers illustrate the decrease in SA as PABA concentration increases. Error bars represent ± SD ($n = 3$). RAUC increases as SA decreases, up to a value of 7, after which the cocrystal dissolution advantage begins to decline. SA values were obtained from the $S_{cocrystal}$ to S_{drug} ratio, further details are included in the supplementary material. (Table S6). Parameters were calculated by considering the final dissolution pH, which lowered with additional PABA (Table 3).

advantage no longer exists. This explains the observed decrease in RAUC under these higher PABA conditions. The conversion of a cocrystal to its drug form occurs faster when cocrystal SA >> drug critical supersaturation threshold, making SA a useful indicator of the driving force for drug precipitation. Since SA predictably decreases with increasing non-stoichiometric coformer concentrations, the correlation shown in Fig. 5 provides valuable insight into how excess coformer influences cocrystal dissolution kinetics.

3.2.3. Measured PABA concentrations during dissolution

A statistically significant decrease in PABA concentrations in the donor after 30 min until the final timepoint ($p < 0.05$) was observed (3.88 mM and above) across the side-by-side experiment, suggesting permeation of PABA through the biomimetic barrier. (Fig. 6) The PABA doses added are below saturation and at pH 6.50, PABA is nearly 1500 times more soluble than KTZ, facilitating rapid dissolution, as observed by the full dissolution of PABA dose within the first 20 min. This is further supported by the absence of PABA in the solid phase at the end of the experiment, as confirmed by XRPD analysis (Fig. S10), indicating no precipitation occurred. The observation of PABA permeation is to be

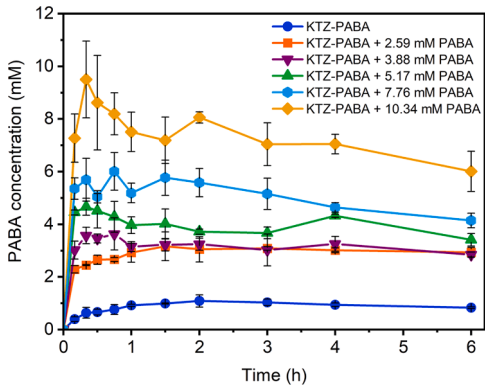

Fig. 6. PABA donor concentration during combined D/P studies of cocrystal with and without excess coformer (2.59, 3.88, 5.17, 7.76 and 10.34 mM) (0–6 h) in FaSSIF pH 6.50. A significant decrease in PABA concentration during KTZ-PABA dissolutions with 3.88 PABA and above was observed within the donor compartment. Standard deviation is represented by error bars ($n = 3$).

expected: PABA exhibits amphoteric behaviour due to its amino and carboxylic acid functional groups with $pK_{a1} = 2.41$ and $pK_{a2} = 4.87$ and a log $P = 0.86$, which contribute to its moderate lipophilicity. (Avdeef, 2012; Hansch et al., 1995) Permeation of PABA through phosphatidylcholine bilayers has been described, as well as fast absorption *in situ* in rats. (Inui et al., 1977; Yamamoto et al., 1991) Furthermore, an *in vivo* rat study conducted by (Kataoka et al., 2021) demonstrated that PABA was rapidly absorbed in the intestinal tract following the administration of three different cocrystals containing PABA as a coformer, including KTZ-PABA.

3.3. Cocrystal DSP in the presence of an absorptive environment: acceptor compartment

The contribution of cocrystal DSP to drug permeation through the PermeaPad® barrier can be examined in Fig. 7, which shows drug concentration profiles over time in the donor compartment (Fig. 7A), along with the corresponding cumulative drug permeation into the acceptor compartment (Fig. 7B). Key findings for KTZ permeation are summarised in Table 4. All cocrystal formulations demonstrate enhanced drug permeation compared to pure crystalline KTZ. The cumulative KTZ permeated into the acceptor at 6 h was 1.6-fold higher for the KTZ–PABA cocrystal than for the pure drug, which is a result of the short-lived supersaturation followed by KTZ precipitation. (Table 4 and Fig. 7A) Cocrystal with additional coformer further improved KTZ permeation for all tested conditions, with the first notable enhancement observed with additional 2.59 mM PABA (5.4-fold). The largest increases in final cumulative concentration were similar for 3.88 mM (7.4-fold) and 5.17 mM PABA (7.3-fold) ($p > 0.05$), although both exhibited different DSP profiles in the donor. For 5.17 mM PABA, the degree of supersaturation was sustained at ~ 4.7, whereas for 3.88 mM PABA supersaturation peaked higher at 6.6 until 0.5 h before declining to ~2.5 by the end of the experiment. This initial higher supersaturation appears to be a key factor driving KTZ diffusion through the barrier. This observation is consistent with (Higashino et al., 2023), who reported that the degree of supersaturation is a more significant determinant of KTZ permeation *in vivo* than its duration (*i.e.*, increased dissolution AUC). For lipophilic drugs such as KTZ, both supersaturation and the presence of drug-rich colloidal species promote rapid absorption. (Frank et al., 2014; Tho et al., 2010)

Cocrystal with the highest added PABA, 7.76 mM and 10.34 mM, resulted in similar KTZ permeation enhancement, with respect to cumulative KTZ by 5.2-fold and 4.5-fold, respectively. ($p > 0.05$) At PABA concentrations higher than 5.17 mM, KTZ permeation enhancement starts to decrease as a result of decreasing cocrystal solubility advantage,

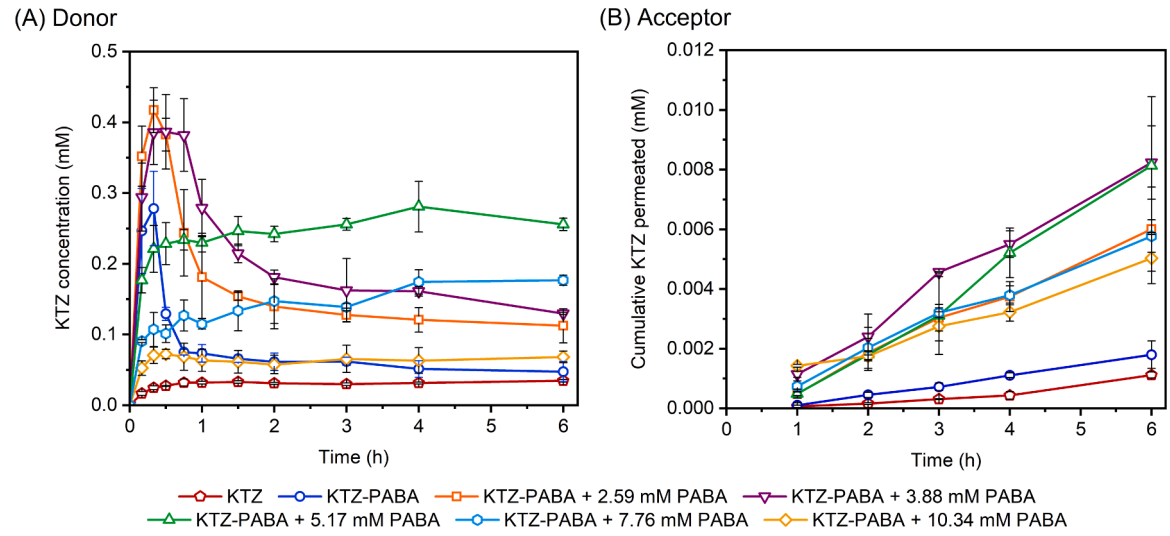

Fig. 7. The modulation of cocrystal DSP translated into enhanced KTZ permeation**.** Combined D/P profiles of pure KTZ and KTZ-PABA cocrystal with 0, 2.59, 3.88, 5.17, 7.76 and 10.34 mM excess PABA performed in side-by-side cells employing a PermeaPad® barrier. (0–6 h) (A) KTZ donor concentrations *vs* time during dissolution in FaSSIF pH 6.50. (B) Cumulative amount of permeated KTZ *vs* time in the acceptor compartment in 2 % w/v Vit E TPGS pH 6.50. KTZ-PABA with excess 3.88 mM and 5.17 mM exhibited superior drug permeation within 6 h in comparison to all other conditions. Error bars for both donor and acceptor compartments represent the standard deviation ($n = 3$).

Table 4
Acceptor compartment key parameters for pure KTZ and KTZ-PABA with and without excess PABA including SD. ($n = 3$) Initial 2 % w/v Vit E TPGS acceptor media pH = 6.50.

Solid phase ($PABA_{added}$)	Cumulative KTZ concentration $(mM)_{6\ h}$ [a] ± SD (10^{-3})	Cumulative KTZ concentration ratio $_{6\ h}$ [b] ± SD	$AUC_{acceptor\ (1–6\ h)}$ (mM.h) ± SD (10^{-3})	$RAUC_{acceptor\ (1–6\ h)}$ [c] ± SD	Total $flux_{(1–6\ h)}$ [d] (μg/(cm^2 x h)) ± SD
KTZ	1.1 ± 0.5	-	2.0 ± 0.2	-	0.281 ± 0.001
KTZ-PABA (0 mM)	1.8 ± 0.5	1.6 ± 0.4	4.8 ± 0.6	2.4 ± 0.3	0.524 ± 0.127
KTZ-PABA (2.59 mM)	6.0 ± 1.4	5.4 ± 0.4	15.9 ± 0.8	7.9 ± 0.4	1.722 ± 0.069
KTZ-PABA (3.88 mM)	8.2 ± 1.2	7.4 ± 0.4	23.7 ± 2.6	11.7 ± 1.3	2.161 ± 0.273
KTZ-PABA (5.17 mM)	8.1 ± 2.3	7.3 ± 0.2	21.9 ± 5.2	10.8 ± 2.6	2.478 ± 0.550
KTZ-PABA (7.76 mM)	5.8 ± 0.5	5.2 ± 0.5	16.9 ± 0.9	8.3 ± 0.5	1.540 ± 0.145
KTZ-PABA (10.34 mM)	5.0 ± 0.8	4.5 ± 0.8	14.8 ± 0.7	7.3 ± 0.4	1.017 ± 0.300

[a] Cumulative KTZ concentration considers samples aliquots from each timepoint (1–6 h).
[b] Cumulative KTZ concentration ratio between cocrystal conditions to pure drug.
[c] RAUC = $AUC_{cocrystal}$ / AUC_{drug}.
[d] Total flux determined as detailed in section 5.6 of supplementary material.

as previously discussed. (Fig. 5) Interestingly, despite generating the same amount of KTZ as pure KTZ-PABA for drug permeation (donor AUC = $p > 0.05$), the 10.34 mM condition exhibited a larger permeation than expected. Permeation profiles of 2.59 mM and 7.76 mM in Fig. 7B showed no statistically significant difference with respect to the final cumulative KTZ. ($p > 0.05$) Despite exhibiting different dissolution kinetics - 2.59 mM with a typical DSP profile and a short-lived high supersaturation, whilst 7.76 mM generated and sustained supersaturation at lower levels of 2.6 - both resulted in the same KTZ AUC values in the donor for compartment permeation. ($p > 0.05$).

These findings offer an opportunity to examine the relationship between the amount of KTZ available in the donor compartment (expressed as the donor AUC) and the extent of permeation, as indicated by the total flux of KTZ into the acceptor. Fig. 8A illustrates the correlation between the two parameters, whilst Fig. 8B allows for visualisation of their trends. A linear correlation ($R^2 = 0.941$) between the two D/P parameters was observed, whereby increases in donor AUC were associated with increases in KTZ total flux. In this study, the donor AUC reflects the total measured KTZ concentration, which is assumed to represent the apparently dissolved fraction. This may include both molecularly dissolved drug and colloidal states, such as drug-rich nanodroplets or micelles. (Frank et al., 2014)

As depicted in Fig. 8A, the increased donor AUC creates a higher driving force for drug permeation as it increases the amount of KTZ available for permeation, consequently increasing flux compared to pure KTZ. However, for pure KTZ-PABA due to rapid drug precipitation within 1 h, the KTZ permeation is not enhanced to the extent of that achieved by cocrystal plus excess coformer. Conditions with highest donor AUC, including 3.88 mM and 5.17 mM, present larger total flux values, compared to those for 2.59 mM and 7.76 mM which present lower donor AUC and corresponding reduced flux. Despite dissolution rate differences, some conditions were equivalent in providing KTZ for delivery across the PermeaPad® barrier (3.88 mM and 5.17 mM as well as 2.59 mM and 7.76 mM).

By examining Fig. 8B, which compares donor AUC and total flux ratios (cocrystal conditions to drug), it is clear the trends for each parameter are mirrored. Both donor AUC and total KTZ flux ratios, increase simultaneously until the 5.17 mM PABA condition, after which

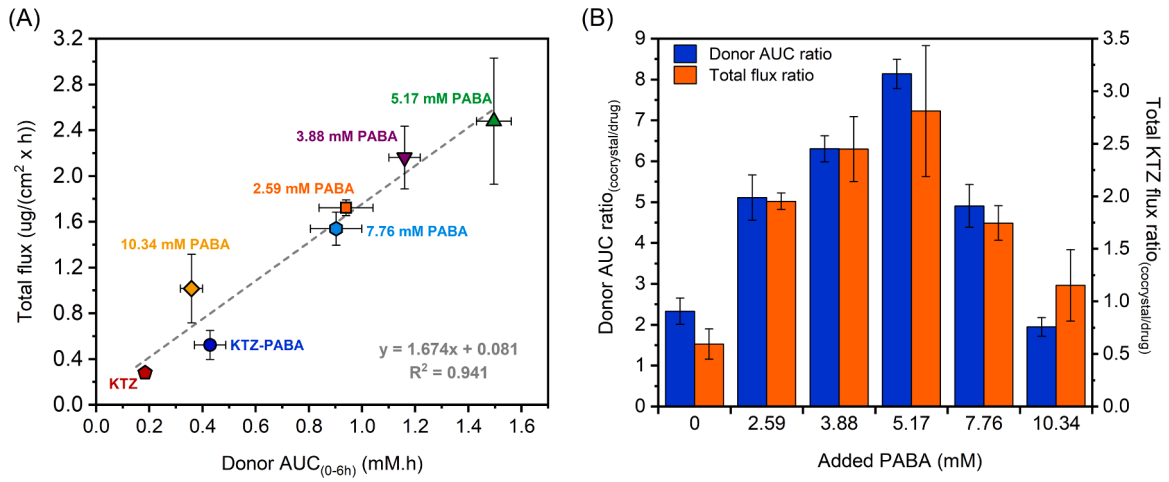

Fig. 8. Correlation between donor AUC (0–6 h) *vs* total flux (1–6 h) of KTZ, expressed in standard parameter units (A) and as the ratio of cocrystal condition to pure KTZ (B). Increases in donor AUC are positively correlated with increases in total flux. Dashed line represents the trendline. ($R^2 = 0.941$) Error bars denote standard deviations across replicates ($n = 3$).

ratios decline, due to diminished cocrystal SA as detailed in Fig. 5. Among all conditions, the 10.34 mM PABA slightly deviates from the overall trend, which correlates kinetic findings in both donor and acceptor. Assuming no active transporters are required, mass transport of poorly soluble drugs like KTZ is facilitated by passive diffusion, driven by a concentration gradient which aids the permeation of KTZ from an area of high to low concentration. Based on this transport mechanism and the donor AUC, a lower KTZ permeation would be expected for the 10.34 mM PABA condition. To the best of the authors knowledge, no evidence indicates that PABA enhances KTZ absorption. (Kataoka et al., 2021)

3.4. Analyzing in vivo outcomes for KTZ-PABA

Earlier studies have investigated the *in vivo* behaviour of KTZ-PABA using rats as the experimental model. (Kataoka et al., 2021; Martin et al., 2020) Kataoka and coworkers administered KTZ-PABA orally in gelatine capsules and reported a substantial enhancement in oral KTZ absorption, with 16.9-fold increase in the AUC (0–8 h) for plasma concentration over time compared to the crystalline pure drug. (Kataoka et al., 2021) While (Martin et al., 2020) observed a 6.7-fold increase in KTZ serum concentration–time profiles when KTZ-PABA was administered in a 0.5 % polyvinylpyrrolidone (PVP) K-30 suspension. PVP is a polymer with solubility enhancing properties, which could have reduced the solubility advantage of the cocrystal over the pure drug, potentially resulting in a lower *in vivo* AUC. (Ban et al., 2020) While both *in vivo* studies exhibited highly increased KTZ absorption, evaluation of the same cocrystal under the present *in vitro* D/P study revealed a 1.6-fold higher cumulative permeation of KTZ at 6 h. The observed quantitative difference in *in vitro-in vivo* (IVIV) predictive performance arises from the distinct parameters each method assesses, together with differences in dynamics, surface area available for permeation, and the extent to which physiological conditions are mimicked.

It is also possible that colloidal species contributed to KTZ *in vivo* absorption in the mentioned studies. As reported by (Higashino et al., 2023), oral absorption of KTZ in rats was significantly enhanced by supersaturated solutions and the presence of liquid–liquid phase separation (LLPS). This phenomenon is likely to occur immediately after cocrystal dissociation and generation of maximum KTZ supersaturation, which, for KTZ–PABA, takes place within a few minutes (t_{max}= 15 min). Although the *in vitro* D/P model used in principle is capable of capturing supersaturation-induced enhanced KTZ permeation contribution induced by colloidal species, the rapid supersaturation of KTZ generated in the donor phase may not have been fully reflected in its permeation into the acceptor, due to the apparent lag time required for the barrier to equilibrate before drug permeation occurs, something that may happen more rapidly *in vivo*. (Nunes et al., 2023a) The rate of KTZ nucleation and crystal growth in the donor may surpass the ability of dissolved KTZ to permeate. In addition, the underestimation of enhanced *in vivo* permeation by the cocrystal may be attributed to the surface-area-to-donor-volume (A/V) ratio of 0.25 cm^{-1} of the D/P model employed, which is substantially lower than human physiological A/V estimated between 1.9 cm^{-1} and 2.3 cm^{-1}. (Mudie et al., 2012) This reduced ratio limits the available surface for drug permeation relative to the volume *in vitro*, potentially leading to an underrepresentation of the cocrystal absorption potential. (O'Shea et al., 2022) An alternative for future assessments is the PermeaLoop™ which offers increased surface area and A/V ratio of 1.38 cm^{-1}. (Nunes et al., 2023b; Sironi et al., 2018) Nevertheless, in the present study, the addition of excess coformer concentrations enhanced drug permeation *in vitro* following cocrystal dissolution, compared to dissolution of cocrystal alone without excess coformer concentrations. This suggests that such excess coformer concentrations may further improve drug absorption *in vivo* relative to the pure cocrystal without added coformer.

3.5. Coformer absorption considerations

There is limited literature on how excess coformer may affect *in vivo* drug absorption following cocrystal administration. In a later publication, (Kataoka et al., 2023) performed an *in vivo* rat study investigating the co-administration of KTZ-PABA (1.26 mg) and excess PABA (2.6 mg). Interestingly, excess PABA reduced KTZ C_{max} from 959.5 ± 233.3 ng/mL (KTZ-PABA) to 560.1 ± 283.7 ng/mL (KTZ-PABA + PABA) and did not improve the overall KTZ exposure due to similar AUC between both conditions (AUC of 1567 ± 133 ng.h/mL for pure KTZ-PABA and 1432 ± 307 ng.h/mL for KTZ-PABA + PABA.) Considering the doses reported by the authors (KTZ-PABA = 1.26 mg and PABA = 2.6 mg) and an administration volume of 1 mL, cocrystal C_{dose} with additional PABA corresponds to C_{dose} = 1.88 mM + 18.96 mM PABA. This dose is significatively higher than the excess PABA concentration analysed in the present study, which does not allow for direct comparison with our *in vitro* D/P findings. It is important to note that the excess PABA dose evaluated *in vivo* by (Kataoka et al., 2023) exceeds the PABA concentrations required to reach the eutectic point for this cocrystal in FaSSIF. Our D/P findings with high concentrations of PABA (7.76 and 10.34 mM) which approach the eutectic, showed a trend of decreased AUC in both the donor and acceptor compartments, indicating that the cocrystal is no longer advantageous in the presence of excessively high coformer

concentrations. This is consistent with the mentioned *in vivo* findings for this cocrystal with excess PABA.

Since the findings presented here show cocrystal DSP and drug permeation are highly dependent on non-stoichiometric solution composition, the absorption properties of the coformer should also be taken into account during cocrystal development. PABA exhibited rapid absorption by the intestinal mucosa in rats, with a t_{max} of 15 min, following its dissociation from the KTZ–PABA cocrystal. (Kataoka et al., 2021) From the *in vitro* D/P findings, it was observed that PABA permeates across the PermeaPad® barrier, as indicated by the decrease in PABA concentrations in the donor compartment (Fig. 6). This raises the question of whether and how coformer absorption could impact cocrystal *in vivo* performance. It is important to note that PABA is an amphoteric compound, whereas many cocrystals involve coformers that are monoprotic acids, whose permeation behaviour may differ significantly. (Singh et al., 2023) Further investigation of cocrystals with coformers of varying lipophilicity is needed to better understand the impacts of coformer on *in vivo* drug absorption.

4. Conclusion

The present study provides insights into the cocrystal dissolution-supersaturation-precipitation behaviour in the presence of an absorptive environment, demonstrating not only that cocrystal has the ability to improve drug permeation, but also that non-stoichiometric coformer concentrations can modulate drug permeation kinetics. Using the *in vitro* side-by-side model equipped with the PermeaPad® barrier enabled detailed characterization of the dynamics of dissolution and permeation for ketoconazole-*p*-aminobenzoic acid cocrystal, revealing a correlation between supersaturation and increased drug flux across the barrier. Notably, addition of excess coformer concentrations in the donor compartment led to increased drug permeation *in vitro* following cocrystal dissolution, compared to conditions without added excess coformer. Additionally, integrating both *in vitro* and *in vivo* findings offered valuable insights into the impact of coformers on cocrystal performance, showing that drug permeation improvements diminish at high excess coformer concentrations. The rational selection of optimal coformer concentrations can be guided by applying the fundamental concepts of cocrystal thermodynamic characterization used in this work, alongside dissolution/permeation (D/P) investigations.

CRediT authorship contribution statement

Lucy May Newman: Writing – review & editing, Writing – original draft, Visualization, Methodology, Investigation, Formal analysis, Conceptualization. **Matteo Guidetti:** Writing – review & editing, Methodology, Investigation, Formal analysis. **Annette Bauer-Brandl:** Writing – review & editing, Methodology. **Naír Rodríguez-Hornedo:** Writing – review & editing, Methodology. **Tatiane Cogo Machado:** Writing – review & editing, Supervision, Project administration, Methodology, Formal analysis, Conceptualization.

Declaration of competing interest

Annette Bauer-Brandl is an inventor of the PermeaPad® barrier, the patent of which is owned and out-licensed by the University of Southern Denmark. The authors report no conflicts of interest.

Acknowledgments

The authors gratefully acknowledge the Engineering and Physical Sciences Research Council (EPSRC) for the funding of this PhD studentship (EP/W524700/1). The authors are grateful for fruitful discussion and collaborations enabled by funding from Nordforsk Program Nordic University Hub (project #85352).

Supplementary materials

Supplementary material associated with this article can be found, in the online version, at doi:10.1016/j.ejps.2025.107426.

Data availability

Data will be made available on request.

References

Avdeef, Alex., 2012. Absorption and Drug Development, 2nd Edition. John Wiley & Sons. https://doi.org/10.1002/9781118286067.

Ban, E., An, S.H., Park, B., Park, M., Yoon, N.E., Jung, B.H., Kim, A., 2020. Improved solubility and oral absorption of emodin-nicotinamide cocrystal over emodin with PVP as a solubility enhancer and crystallization inhibitor. J. Pharm. Sci. 109 (12), 3660–3667. https://doi.org/10.1016/j.xphs.2020.09.030.

Bibi, H.A., Holm, R., Bauer-Brandl, A., 2017. Simultaneous lipolysis/permeation in vitro model, for the estimation of bioavailability of lipid based drug delivery systems. Euro. J. Pharma. Biopharm. 117, 300–307. https://doi.org/10.1016/J.EJPB.2017.05.001.

Buckley, S.T., Frank, K.J., Fricker, G., Brandl, M., 2013. Biopharmaceutical classification of poorly soluble drugs with respect to "enabling formulations in". In: Euro. J. Pharma. Sci., 50. Elsevier B.V., pp. 8–16. https://doi.org/10.1016/j.ejps.2013.04.002

Cavanagh, K.L., Kuminek, G., Rodríguez-Hornedo, N., 2020. Cocrystal solubility advantage and dose/solubility ratio diagrams: a mechanistic approach to selecting additives and controlling dissolution-supersaturation-precipitation behavior. Mol. Pharm. 17 (11), 4286–4301. https://doi.org/10.1021/acs.molpharmaceut.0c00713.

Dai, X.L., Li, S., Chen, J.M., Lu, T.B., 2016. Improving the membrane permeability of 5-fluorouracil via cocrystallization. Cryst. Growth Desi. 16 (8), 4430–4438. https://doi.org/10.1021/acs.cgd.6b00552.

Di Cagno, M., Bibi, H.A., Bauer-Brandl, A., 2015. New biomimetic barrier Permeapad™ for efficient investigation of passive permeability of drugs. Euro. J. Pharma. Sci. 73, 29–34. https://doi.org/10.1016/j.ejps.2015.03.019.

Eriksen, J.B., Messerschmid, R., Andersen, M.L., Wada, K., Bauer-Brandl, A., Brandl, M., 2020. Dissolution/permeation with PermeaLoop™: experience and IVIVC exemplified by dipyridamole enabling formulations. Euro. J. Pharma. Sci. 154, 105532. https://doi.org/10.1016/j.ejps.2020.105532.

Fong, S.Y.K., Bauer-Brandl, A., Brandl, M., 2017. Oral bioavailability enhancement through supersaturation: an update and meta-analysis in. In: Expert Opinion on Drug Delivery, 14. Taylor and Francis Ltd, pp. 403–426. https://doi.org/10.1080/17425247.2016.1218465.

Frank, K.J., Westedt, U., Rosenblatt, K.M., Hölig, P., Rosenberg, J., Mägerlein, M., Fricker, G., Brandl, M., 2014. What is the mechanism behind increased permeation rate of a poorly soluble drug from aqueous dispersions of an amorphous solid dispersion? J. Pharm. Sci. 103 (6), 1779–1786. https://doi.org/10.1002/jps.23979.

Good, D.J., Naír, R.H., 2009. Solubility advantage of pharmaceutical cocrystals. Cryst. Growth Desi. 9 (5), 2252–2264. https://doi.org/10.1021/cg801039j.

Groom, C.R., Bruno, I.J., Lightfoot, M.P., Ward, S.C., 2016. The Cambridge Structural Database. CSD. https://doi.org/10.1107/S2052520616003954.

Guidetti, M., 2024. Doctoral, Dissertation. University of Southern DenmarkSyddansk Universitet. https://doi.org/10.21996/xazq-sr30.

Guo, M., Wang, K., Qiao, N., Yardley, V., Li, M., 2018. Investigating permeation behavior of flufenamic acid cocrystals using a dissolution and permeation system. Mol. Pharm. 15 (9), 4257–4272. https://doi.org/10.1021/acs.molpharmaceut.8b00670.

Hansch, C., Hoekman, D., Leo, A., Zhang, L., Li, P., 1995. The expanding role of quantitative structure-activity relationships (QSAR) in toxicology. Toxicol. Lett. 79 (1–3), 45–53. https://doi.org/10.1016/0378-4274(95)03356-P.

Higashino, H., Minami, K., Takagi, T., Kataoka, M., Yamashita, S., 2023. The effects of degree and duration of supersaturation on in vivo absorption profiles for highly permeable drugs, dipyridamole and ketoconazole. Euro. J. Pharma. Biopharma. 189 (June), 48–55. https://doi.org/10.1016/j.ejpb.2023.06.002.

Holzem, F.L., Jensen, I.H., Petrig Schaffland, J., Stillhart, C., Brandl, M., Bauer-Brandl, A., 2023. Combining in vitro dissolution/permeation with microdialysis sampling: capabilities and limitations for biopharmaceutical assessments of supersaturating drug formulations. Euro. J. Pharma. Sci. 188. https://doi.org/10.1016/j.ejps.2023.106533.

Holzem, F.L., Weck, A., Schaffland, J.P., Stillhart, C., Klein, S., Bauer-Brandl, A., Brandl, M., 2022. Biopredictive capability assessment of two dissolution/permeation assays, μFLUX™ and PermeaLoop™, using supersaturating formulations of Posaconazole. Euro. J. Pharma. Sci. 176. https://doi.org/10.1016/j.ejps.2022.106260.

Huang, Y., Kuminek, G., Roy, L., Cavanagh, K.L., Yin, Q., Rodríguez-Hornedo, N., 2019. Cocrystal solubility advantage diagrams as a means to control dissolution, supersaturation, and precipitation. Mol. Pharm. 16 (9), 3887–3895. https://doi.org/10.1021/acs.molpharmaceut.9b00501.

Ilie, A.R., Griffin, B.T., Brandl, M., Bauer-Brandl, A., Jacobsen, A.C., Vertzoni, M., Kuentz, M., Kolakovic, R., Holm, R., 2020. Exploring impact of supersaturated lipid-based drug delivery systems of celecoxib on in vitro permeation across Permeapad® membrane and in vivo absorption. Euro. J. Pharma. Sci. 152, 105452. https://doi.org/10.1016/J.EJPS.2020.105452.

Inui, K.-I, Tabara, K., Hori, R., Kaneda, A., Muranishi, S., Sezaki, H., 1977. Black lipid membranes as a model for intestinal absorption of drugs. J. Pharma. Pharma. 29 (1), 22–26. https://doi.org/10.1111/j.2042-7158.1977.tb11231.x.

Jacobsen, A.C., Visentin, S., Butnarasu, C., Stein, P.C., di Cagno, M.P., 2023. Commercially available cell-free permeability tests for industrial drug development: increased sustainability through reduction of in vivo studies. In: Pharmaceutics, 15. MDPI. https://doi.org/10.3390/pharmaceutics15020592.

Kataoka, M., Minami, K., Takagi, T., Amidon, G.E., Yamashita, S., 2021. In vitro-In vivo correlation in cocrystal dissolution: consideration of drug release profiles based on coformer dissolution and absorption behavior. Mol. Pharm. 18 (11), 4122–4130. https://doi.org/10.1021/acs.molpharmaceut.1c00537.

Kataoka, M., Yonehara, A., Minami, K., Takagi, T., Yamashita, S., 2023. Control of dissolution and supersaturation/precipitation of poorly water-soluble drugs from cocrystals based on solubility products: a case study with a ketoconazole cocrystal. Mol. Pharm. 20 (8), 4100–4107. https://doi.org/10.1021/acs.molpharmaceut.3c00237.

Kuminek, G., Cao, F., Bahia de Oliveira da Rocha, A., Gonçalves Cardoso, S., Rodríguez-Hornedo, N., 2016. Cocrystals to facilitate delivery of poorly soluble compounds beyond-rule-of-5. Adv. Drug Deliv. Rev. 101, 143–166. https://doi.org/10.1016/j.addr.2016.04.022.

Lukács, M., Barcsa, G., Kovács-Hadady, K., 1998. The effects of pH, ionic strength and buffer concentration of mobile phase on RF of acidic compounds in ion-pair TLC. Chromatographia 48, 511516. https://doi.org/10.1007/BF02466642.

Machado, T.C., Kavanagh, O.N., Cardoso, S.G., Rodríguez-Hornedo, N., 2022. Synchronization of cocrystal dissolution and drug precipitation to sustain drug supersaturation. Mol. Pharm. 19 (8), 2765–2775. https://doi.org/10.1021/acs.molpharmaceut.2c00122.

Machado, T.C., Kuminek, G., Cardoso, S.G., Rodríguez-Hornedo, N., 2020. The role of pH and dose/solubility ratio on cocrystal dissolution, drug supersaturation and precipitation. Euro. J. Pharma. Sci. 152 (June), 105422. https://doi.org/10.1016/j.ejps.2020.105422.

Martin, F., Pop, M., Kacso, I., Grosu, I.G., Miclăuş, M., Vodnar, D., Lung, I., Filip, G.A., Olteanu, E.D., Moldovan, R., Nagy, A., Filip, X., Băldea, I., 2020. Ketoconazole- p-aminobenzoic acid cocrystal: revival of an old drug by crystal engineering. Mol. Pharm. 17 (3), 919–932. https://doi.org/10.1021/acs.molpharmaceut.9b01178.

Mudie, D.M., Shi, Y., Ping, H., Gao, P., Amidon, G.L., Amidon, G.E., 2012. Mechanistic analysis of solute transport in an in vitro physiological two-phase dissolution apparatus. Biopharma. Drug Disposit. 33 (7), 378–402. https://doi.org/10.1002/bdd.1803.

Nehm, S.J., Rodríguez-Spong, B., Rodríguez-Hornedo, N., 2006. Phase solubility diagrams of cocrystals are explained by solubility product and solution complexation. Cryst. Growth. Desi. 6 (2), 592–600. https://doi.org/10.1021/cg0503346.

Newman, L.M., Kavanagh, O.N., Machado, T.C., 2025. DSPindex guides dose selection to extend drug supersaturation lifetime during cocrystal dissolution. Int. J. Pharm. 671. https://doi.org/10.1016/j.ijpharm.2025.125298.

Nunes, P.D., Ferreira, A.F., Pinto, J.F., Bauer-Brandl, A., Brandl, M., Henriques, J., Paiva, A.M., 2023a. In vitro dissolution/permeation tools for amorphous solid dispersions bioavailability forecasting II: comparison and mechanistic insights. Euro. J. Pharma. Sci. 188, 106513. https://doi.org/10.1016/J.EJPS.2023.106513.

Nunes, P.D., Pinto, J.F., Bauer-Brandl, A., Brandl, M., Henriques, J., Paiva, A.M., 2023b. In vitro dissolution/permeation tools for amorphous solid dispersions bioavailability forecasting i: experimental design for PermeaLoop™. Euro. J. Pharma. Sci. 188. https://doi.org/10.1016/j.ejps.2023.106512.

O'Shea, J.P., Augustijns, P., Brandl, M., Brayden, D.J., Brouwers, J., Griffin, B.T., Holm, R., Jacobsen, A.C., Lennernäs, H., Vinarov, Z., O'Driscoll, C.M, 2022. Best practices in current models mimicking drug permeability in the gastrointestinal tract - an UNGAP review. Euro. J. Pharma. Sci. 170, 106098. https://doi.org/10.1016/J.EJPS.2021.106098.

Pandey, N., Ghosh, A., 2022. An outlook on permeability escalation through cocrystallization for developing pharmaceuticals with improved biopharmaceutical properties. In: Journal of Drug Delivery Science and Technology, 76. Editions de Sante. https://doi.org/10.1016/j.jddst.2022.103757.

Rodríguez Hornedo, Naír, Nehm, S.J., Seefeldt, K.F., Pagán-Torres, Y., Falkiewicz, C.J, 2006. Reaction crystallization of pharmaceutical molecular complexes. Mol. Pharm. 3 (9), 8456–8457. https://doi.org/10.1021/mp050099m.

Sanphui, P., Devi, V.K., Clara, D., Malviya, N., Ganguly, S., Desiraju, G.R., 2015. Cocrystals of hydrochlorothiazide: solubility and diffusion/permeability enhancements through drug-coformer interactions. Mol. Pharm. 12 (5), 1615–1622. https://doi.org/10.1021/acs.molpharmaceut.5b00020.

Schver, G.C.R.M., Lee, P.I., 2018. Combined effects of supersaturation rates and doses on the kinetic-solubility profiles of amorphous solid dispersions based on water-insoluble poly(2-hydroxyethyl methacrylate) hydrogels. Mol. Pharm. 15 (5), 2017–2026. https://doi.org/10.1021/acs.molpharmaceut.8b00162.

Singh, M., Barua, H., Jyothi, V.G.S.S., Dhondale, M.R., Nambiar, A.G., Agrawal, A.K., Kumar, P., Shastri, N.R., Kumar, D., 2023. Cocrystals by design: a rational coformer selection approach for tackling the API problems. Pharmaceutics. 15 (4), 1161. https://doi.org/10.3390/PHARMACEUTICS15041161/S1.

Sironi, D., Rosenberg, J., Bauer-Brandl, A., Brandl, M., 2018. PermeaLoop™, a novel in vitro tool for small-scale drug-dissolution/permeation studies. J. Pharm. Biomed. Anal. 156, 247–251. https://doi.org/10.1016/J.JPBA.2018.04.042.

Stillhart, C., Kuentz, M., 2016. Trends in the assessment of drug supersaturation and precipitation in vitro using lipid-based delivery systems. J. Pharm. Sci. 105 (9), 2468–2476. https://doi.org/10.1016/j.xphs.2016.01.010.

Sun, D.D., Lee, P.I., 2015. Haste makes waste: the interplay between dissolution and precipitation of supersaturating formulations. AAPS J. 17 (6), 1317–1326. https://doi.org/10.1208/s12248-015-9825-6.

Tho, I., Liepold, B., Rosenberg, J., Maegerlein, M., Brandl, M., Fricker, G., 2010. Formation of nano/micro-dispersions with improved dissolution properties upon dispersion of ritonavir melt extrudate in aqueous media. Euro. J. Pharma. Sci. 40 (1), 25–32. https://doi.org/10.1016/j.ejps.2010.02.003.

Yamamoto, A., Sakane, T., Shibukawa, M., Hashida, M., Sezaki, H., 1991. Absorption and metabolic characteristics of p-aminobenzoic acid and its isomer, m-aminobenzoic acid, from the rat small intestine. J. Pharm. Sci. 80 (11), 1067–1071. https://doi.org/10.1002/JPS.2600801114.